ACS APPLIED MATERIALS & INTERFACES

Research Article

www.acsami.org

Green Synthesis of Low-Toxicity Graphene-Fulvic Acid with an Open Band Gap Enhances Demethylation of Methylmercury

Xiangang Hu,[†] Li Mu,[‡] Kaicheng Lu,[†] Jia Kang,[†] and Qixing Zhou*[,†]

[†]Key Laboratory of Pollution Processes and Environmental Criteria (Ministry of Education), Tianjin Key Laboratory of Environmental Remediation and Pollution Control, College of Environmental Science and Engineering, Nankai University, Tianjin 300071, China

[‡]Institute of Agro-environmental Protection, Ministry of Agriculture, Tianjin 300191, China

Supporting Information

ABSTRACT: The demethylation of methylmercury has received substantial attention. Here, a novel chemical method for the demethylation of methylmercury is proposed. The low-toxicity graphene-fulvic acid (FA, a ubiquitous material in the environment) was synthesized without the use of a chemical reagent. The hybridized graphene-FA presented an indirect open band gap of 2.25−2.87 eV as well as adequate aqueous dispersion. More importantly, the hybridized graphene-FA exhibited 6- and 10-fold higher photocatalytic efficiencies for the demethylation of methylmercury than FA and free FA with graphene, respectively. This result implies that immobilized, rather than free, FA accelerated the catalysis. Furthermore, inorganic mercuric ion, elemental mercury, and mercuric oxide were identified as the primary demethylation products. For free FA with graphene, graphene quenches the excited-state FA, inhibiting the demethylation by electron transfer. In contrast, the graphene of the self-assembled graphene-FA serves as an electron reservoir, causing electron−hole pair separation. Graphene-FA showed a negligible toxicity toward microalgae compared to graphene. The above results reveal that the green synthesis of graphene and organic molecules is a convenient strategy for obtaining effective cocatalysts.

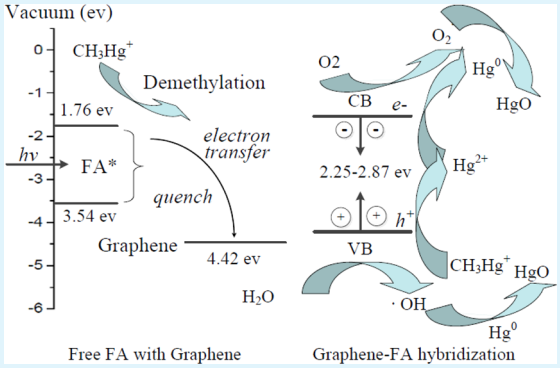

KEYWORDS: *graphene, fulvic acid, methylmercury, graphene oxide, demethylation*

INTRODUCTION

Methylmercury (MeHg) exhibits substantial neurotoxicity, genotoxicity, and reproductive toxicity and poses significant health risks to humans.[1,2] The most commonly used strategies to remove mercury from the environment involve sorption, ion exchange, precipitation, and electrochemical techniques; however, these techniques are insufficient for demethylation or they generate secondary contamination.[3] The demethylation of MeHg in aquatic environments is hypothesized to occur primarily via microbial processes.[4] The novel chemical demethylation of methylmercury through photolysis is considered an effective method to reduce the risks of MeHg, especially when nanomaterials are used as photocatalysts.[4,5] Titanium dioxide (TiO_2), nanotubes, and activated carbon as catalysts have shown excellent capabilities for removing elemental mercury or inorganic mercury.[6,7] Compared to TiO_2, nanotubes, and activated carbon, two-dimensional graphene exhibits a large surface area, excellent catalytic capacity, and good biocompatibility.[8−10]

However, the valence and conduction bands formed meet at the Brillouin zone corners, which makes graphene a zero band gap semiconductor with a limited ability to photocatalyze pollutant degradation.[11] Many researchers have attempted chemical modifications to open the band gap, for example, by coupling graphene with organic molecules or with metal nanoparticles.[5,12]

Three challenges remain regarding graphene-related hybridization.[9,10,13] The first challenge is to find a convenient and economical strategy to open the band gap by chemical modification. Covalent immobilization or coupling with metals or organic molecules requires precious metals, complex fabrication techniques, and numerous chemical reagents, which is not compatible with low-carbon chemistry. The second challenge is to elucidate the mechanisms of cooperation between graphene and chemical modifiers. Whether graphene is a reaction quencher or a reaction promoter remains an unresolved issue. The roles of energy transfer and electron transfer between graphene-based cocatalysts are also obscure. The third challenge is to overcome the aggregation of nanomaterials in aqueous environments due to their large surface energies. Fulvic acid (FA) is the main species of ubiquitous humic substances in the environment.[14,15] The surface hydroxyl, carboxyl, and aromatic groups of FA may interact with sp^2 graphene through $\pi-\pi$ interactions or other

Received: March 6, 2014
Accepted: May 22, 2014
Published: May 22, 2014

noncovalent bonds. To our knowledge, there are no prior reports related to graphene with FA as a cocatalyst for photocatalysis. If ubiquitous FA is immobilized on graphene through a convenient self-assembly approach, the band gap may be opened, and aqueous dispersion may be enhanced.

Therefore, in this work, the hybridization of FA and graphene was investigated as a plausible technique for the photocatalysis of MeHg, and special attention was directed to the catalytic mechanisms. First, graphene-FA was synthesized without any chemical reagents, and its stability was characterized using Fourier transform infrared spectroscopy (FTIR), nuclear magnetic resonance (NMR), X-ray photoelectron spectroscopy (XPS), dynamic light scattering (DLS), and *Zeta* potential measurements. Then, the efficiencies of graphene, FA, free FA with graphene, and hybridized graphene-FA for the photocatalytic demethylation of MeHg were investigated. Furthermore, the photocatalysis products and possible transformation paths were identified by gas chromatography−mass spectrometry/mass spectrometry (GC-MS/MS). Finally, the open band gap, quenching effect, reactive oxygen species (ROS), excited states, electron−hole pairs, electron transfer, and energy transfer were examined to elucidate the associated cocatalysis mechanisms. Finally, it was determined that graphene-FA exhibited negligible toxicity to aquatic algae compared to graphene. This work proposes that the green synthesis of low-toxicity graphene-FA may be a convenient and effective strategy to treat organometal contamination.

EXPERIMENTAL SECTION

Materials. Graphene nanosheets (purity of 99%) were obtained from the Nanjing XFNANO Materials Tech Co., Ltd., China. The single-layer graphene was reduced graphene oxide and was prepared by thermal exfoliation reduction and hydrogen reduction. MeHg and other mercuric species standards were purchased from the Shanghai ANPEL Scientific Instrument Co., Ltd. FA (analytical grade) was purchased from the Shanghai Hui Cheng Biological Technology Co., Ltd. Other chemical reagents were of chromatography or analytical grade.

Green Synthesis of Graphene-FA. A FA solution (50 mL, 150 mg/L, adjusted to pH = 7.0) was prepared and then gently mixed with 0.01 g of graphene for 24 h under darkness. Next, the suspension was centrifuged (3500*g*, 30 min) and filtered (0.2 μm polytetrafluoroethylene membrane) to collect the hybridized graphene-FA, which was then gently rinsed with water. The amount of immobilized FA (112 mg/g) was calculated based on the free FA in the aqueous phase. Various techniques were used to characterize the self-assembled graphene. FTIR spectra were recorded on a Bruker Tensor 27 infrared spectrometer with a resolution of 2 cm^{-1} at 3500−1000 cm^{-1}. Mixtures containing 2 mg of samples ground with 198 mg of KBr (spectroscopy grade) were compressed into transparent pellets for measurement. To confirm the formation of hybridized graphene-FA, solid-state ^{13}C NMR was employed to characterize the structural composition of graphene-FA and FA. Solid-state ^{13}C cross-polarization/magic-angle spinning (CP/MAS) NMR spectra were recorded at 9.4 T using a Varian Infinity Plus-400 spectrometer equipped with a 4 mm MAS probe. The UV−vis spectra of all samples were recorded on a T90 spectrophotometer (Purkinje General, Beijing) equipped with UVW5 software in a 1 cm path length quartz cuvette at 190−600 nm. XPS measurements were performed using an Axis Ultra XPS system (Kratos) with a monochromatic Al Kα X-ray source (1486.6 eV). The spectra were analyzed using CasaXPS v2.3.13 software. The peak deconvolutions were performed using Gaussian components after a Shirley background subtraction.

Aqueous Dispersion of Graphene-FA. The aggregation of the pristine graphene and graphene-FA suspensions was characterized by monitoring the average hydrodynamic diameter using DLS. The hydrodynamic diameter was determined at a constant pH value (pH = 7.0) on a *ZetaPALS* equipped with a 30 mW 657 nm laser (Brookhaven Instruments Corporation, Holtsville, NY, USA). The data were collected for 10 min at intervals of 30 s. *Zeta* potential was measured at pH 3−8 using a Zhongchen JS94H (Shanghai, China). Before all of the hydrodynamic diameter and *Zeta* potential measurements, the samples were dispersed using an ultrasonic probe for 2 min.

Mercury Demethylation. MeHg (1 mg) was reacted with 10 mg/L graphene, FA, free FA with graphene (mass ratio of 112 to 1000), or self-assembled hybridized graphene-FA in a 50 mL suspension under UVA irradiation. UVA irradiation (300−400 nm wavelength) is the main component (95−98%) of UV light in the solar spectrum and is used widely in photochemical tests. In all of the irradiation experiments, black lamps (λ = 365 nm, 15 W, Cnlight Co., Ltd., Guangdong, China) provided 2.3 mW/cm^2 of light intensity on the surfaces of the samples; this intensity is comparable to the UVA intensity measured at ground level on sunny summer days in central China. To investigate the photocatalytic capacity under visible light conditions, a subexperiment was conducted. The suspension was irradiated using a 350−780 nm LED (light-emitting diode) lamp (Cnlight Co., Ltd., Guangdong, China), and the same light intensity was used for UVA irradiation. Prior to the experiment, the lamp was turned on for 30 min to obtain a constant light intensity. To investigate the kinetics of demethylation, irradiation was conducted for 0−300 min with gentle agitation at 300 rpm. To remove the adsorbed mercury ions and mercuric oxide and to regenerate the catalyst, consecutive photocatalysis-regeneration cycles were repeated 10 times using the same catalyst. The regeneration of graphene-HA was conducted according to the literature but with a slight modification.[16] The desorption of mercury ions and mercuric oxide was performed with a 0.1 mol L^{-1} HCl solution. The catalyst loaded with mercury was placed in the desorption medium and stirred for 12 h at 150 rpm at 30 ± 2 °C. Subsequently, graphene was separated through a 0.22 μm filter and reacted with FA to obtain graphene-FA according to the above synthesis.

Identification of Demethylation Products and ROS. Elemental mercury (Hg^0) was continuously collected by purging N_2 through the reactor according to a previously described method.[17] The measurement was performed using GC-MS/MS (Agilent 5976 quadrupole mass spectrometric detector, DB-5 MS separator column) with a sensitivity of 10 $\mu g/m^3$. The adsorbed mercuric species were removed from the graphene-FA by washing with 0.1 M HCl. Following the method of Zachariadis and Kapsimali,[18] the concentrations of CH_3Hg^+, Hg^{2+}, and HgO were directly monitored by GC-MS/MS with limits of detection of 1, 0.5, and 5 μg/L, respectively. The reactions were performed in triplicate, and the error bars represent the standard deviation. Based on various previously reported methods,[5,19] the excited molecules and ROS were analyzed using excess quenchers (dissolved oxygen for excited molecules, sodium azide for singlet oxygen, isopropyl alcohol for hydroxyl radicals, and superoxide dismutase for superoxide anion).

***Chlorella vulgaris* Cultivation.** *Chlorella vulgaris* and its culture medium (BG-11) were purchased from the Freshwater Algae Culture Collection at the Institute of Hydrobiology, China. All materials that contacted microalgae were sterilized. A suspension of 1×10^5 cells/mL was exposed to graphene-FA (100, 10, and 1 mg/L). Graphene (100, 10, and 1 mg/L) and a blank, which was not exposed to grapheme, were used as the controls. The suspensions were shaken once every 8 h and placed in a light incubator for 6 days with 3000 Lx irradiation at 24 °C, and 80% humidity. Cell counting was performed on an inverted fluorescent microscope (CKX41). The chlorophyll a contents were detected using UV−vis spectroscopy.

RESULTS AND DISCUSSION

Characteristics of Self-Assembled Graphene-FA. The physicochemical properties of graphene are provided in the Supporting Information (Table S1 and Figures S1−S4). The

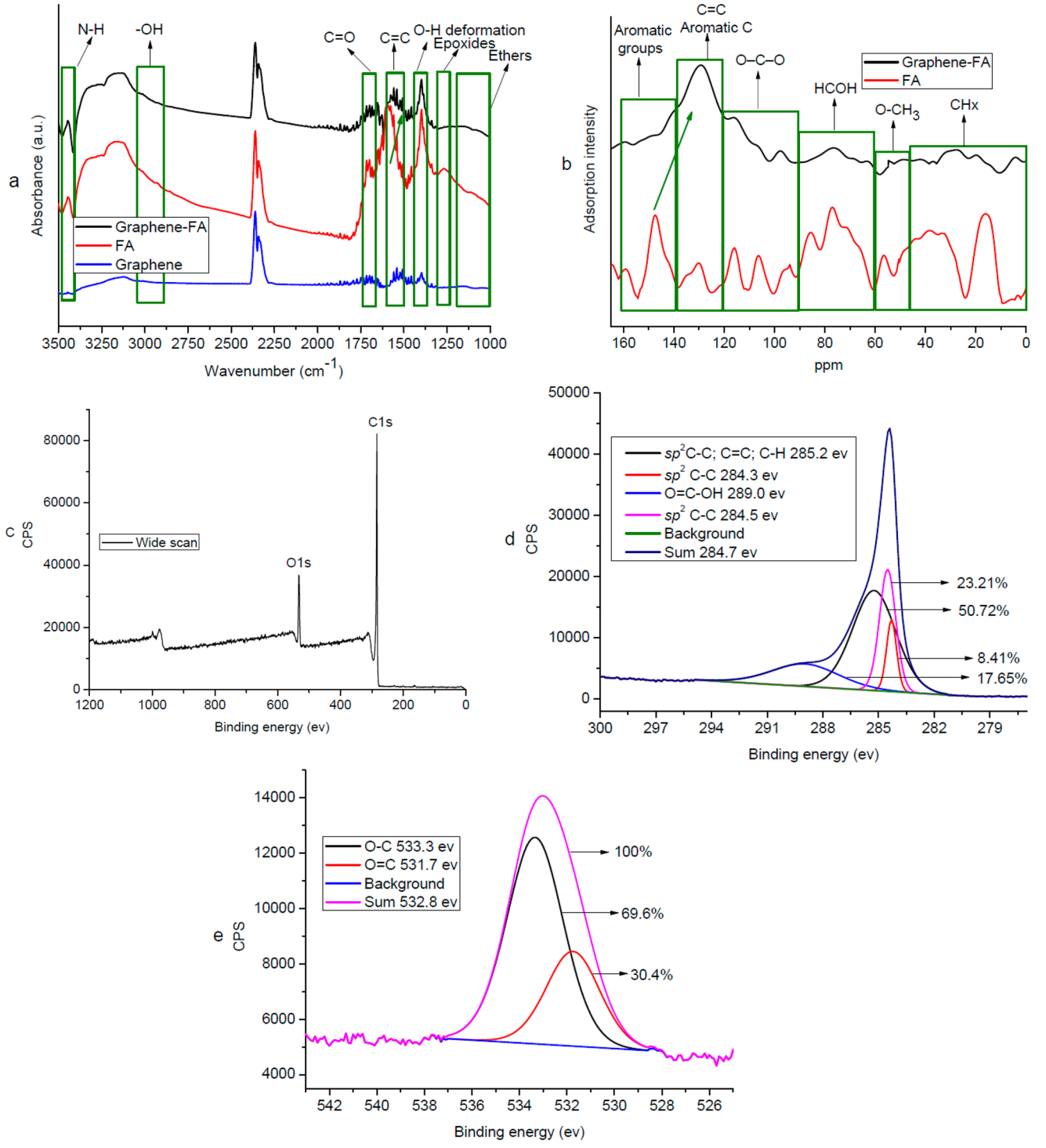

Figure 1. Characteristics of self-assembled graphene-FA. FTIR spectra (a), solid-state ^{13}C NMR spectra (b), and wide scan (c), C 1s (d), and O 1s (e) XPS spectra of graphene-FA.

thickness of the graphene is approximately 0.8 nm, and the diameter of the graphene sheets is approximately 0.5−2 μm, as shown in the atomic force microscopy images. Graphene exhibited a translucent sheet structure with wrinkles around the edges in the high-resolution transmission electron microscopy image. The specific FTIR wavenumbers of graphene and FA were attributed to the corresponding chemical groups referred to in previous reports.[20,21] As presented in Figure 1a, the C═C stretching vibrations were centered at 1600−1500 cm^{-1} for the sp^2 graphene, and weak oxygen-containing groups (−OH and C═O) were also observed in the graphene sample. The limited oxygen groups were attributed to defects in the graphene, particularly defects located on the edge.[20] In contrast, the FTIR spectrum of graphene-FA exhibited strong peaks corresponding to oxygen-containing groups as well as peaks corresponding to new functional groups, such as N−H, epoxides, and ethers. Compared with the spectrum of FA, the C═C groups of graphene-FA presented a blue shift of approximately 40 cm^{-1}, suggesting that the self-assembly was located on the sp^2 plane of graphene. To confirm the hybridization of graphene-FA,

dx.doi.org/10.1021/am501334j | ACS Appl. Mater. Interfaces 2014, 6, 9220−9227

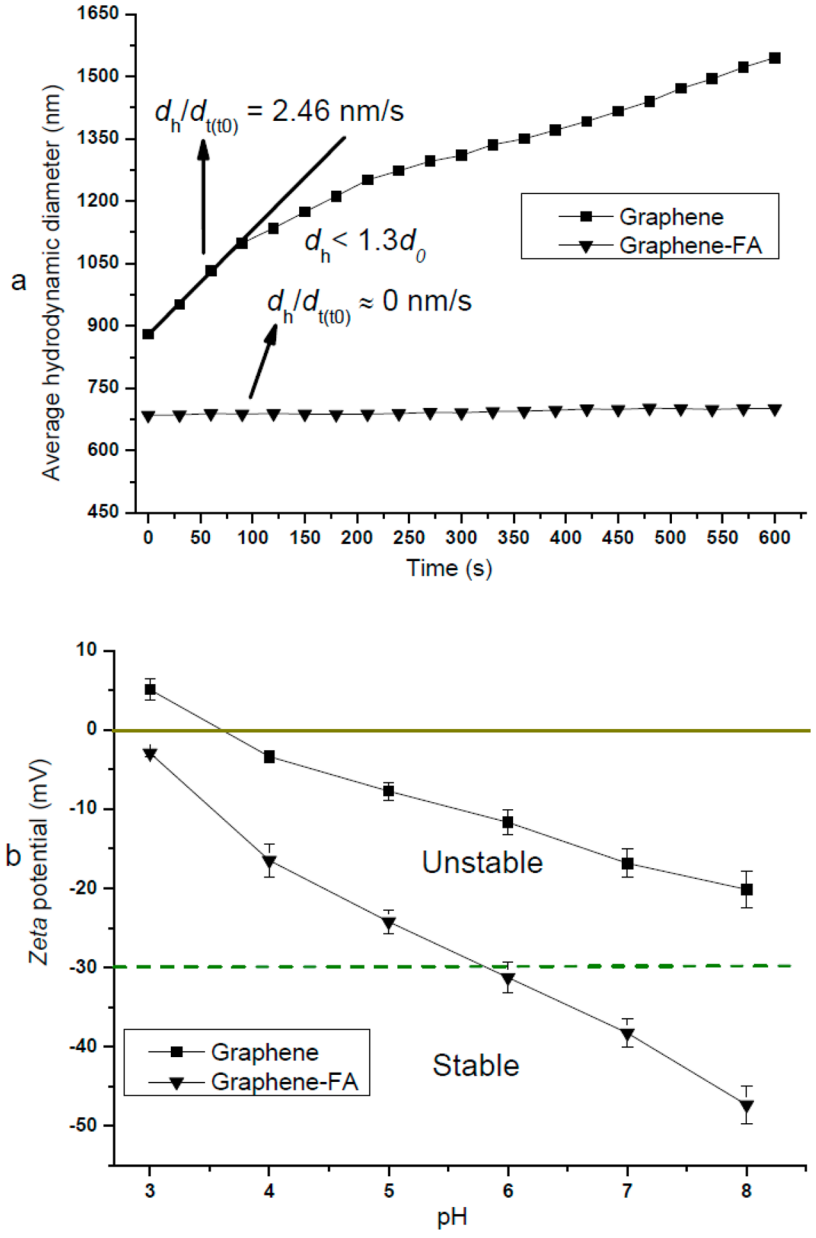

Figure 2. Aqueous dispersion of graphene and graphene-FA. Time profile of average hydrodynamic diameter at pH = 7.0 (a) and variation in *Zeta* potential versus pH (b).

solid-state ^{13}C NMR was conducted. NMR has been widely used in FA structural studies;[22] naked graphene cannot be measured using solid-state ^{13}C NMR due to its intrinsic electrical conductivity. The ^{13}C NMR spectrum of graphene-FA revealed HCOH and O−C−O, especially C═C and aromatic C peaks, indicating that FA was immobilized on the graphene, as shown in Figure 1b. The aromatic groups of FA at 160−140 ppm shifted to 140−120 ppm for graphene-FA, suggesting that the aromatic groups of FA coupled with the graphene sp^2 structure through $\pi-\pi$ interactions, which was consistent with the FTIR results.

XPS was employed as a more optimal characterization technique to provide direct evidence for the conjugation of graphene with FA. As depicted in Figure 1c and d, the deconvoluted peak centered at 284.5 eV is attributed to sp^2 C−C from graphene[23] and accounted for 50.72% of the C 1s spectrum. The peak centered at 289.0 eV, which is attributed to O═C−OH, should be from FA. Compared to the reported peaks at 284.5 (sp^2 C−C, C═C, and C−H) and 285.4 eV (C−C),[24] the peaks centered at 284.3 and 285.2 eV presented a 0.2 eV shift, likely due to the interactions between graphene and FA. The O 1s spectrum is a complement of the C 1s spectrum,[25] as shown in Figure 1e. The peaks centered at 533.3 and 531.7 eV can be attributed to O−C and O═C, respectively. In addition, there were no obvious peaks centered at 530−530.2 eV, which is attributed to bulk O^{2-}, suggesting that graphene oxide (graphene=O) did not form and that the observed oxygen groups were from FA.

Aqueous Dispersion of Graphene-FA. The aqueous dispersion or stability determines the adsorption and photocatalysis efficiencies of nanomaterials, and graphene is no exception.[5,8] DLS and the *Zeta* potential have been widely used to measure the stability of graphene.[26] Notably, graphene or graphene-based materials are aspheric dimensional nanoma-

dx.doi.org/10.1021/am501334j | ACS Appl. Mater. Interfaces 2014, 6, 9220−9227

terials, and the DLS and *Zeta* potential results provide the relevant size distribution. Previous work has suggested that the average hydrodynamic diameter from DLS represents the lateral size rather than the thickness of graphene.[27] The aggregation kinetics were determined using the initial aggregation rate obtained by calculating the initial slope to the point where the hydrodynamic diameter (d_h) reaches 1.3-fold more than the initial hydrodynamic diameter (d_{h0}).[28] As shown in Figure 2a, graphene is unstable in aqueous solution, and its size increased over time, exhibiting an initial aggregation rate of 2.46 nm/s. In contrast, hybridized graphene-FA showed no obvious changes in its hydrodynamic diameters during the testing periods. The *Zeta* potential confirms these results, as presented in Figure 2b. The *Zeta* potential became negative as the pH of the suspension increased, suggesting that the surfaces of graphene and graphene-FA acquired negative charges. FA has an abundance of negatively charged carboxylic and phenolic functional groups. Therefore, coating the surface of graphene with FA enhanced the electrostatic repulsion and steric repulsion among graphenes.[29,30]

FA is negatively charged in the pH range of 4–8.[31] Figure 2b demonstrates that graphene is also negatively charged at pH 4–8. In the neutral solutions used in this study, there is considerable charge repulsion between graphene and FA. To overcome this charge repulsion, FA with aromatic moieties was expected to strongly interact with the graphene surface via van der Waals forces and $\pi-\pi$ stacking, thus predisposing most compounds to lie flat on the basal plane of graphene.[32,33] The shifts in the FTIR and ^{13}C NMR spectra (Figures 1a and b) confirmed that FA coupled with the graphene sp^2 structure through $\pi-\pi$ interactions. The intermolecular electrostatic repulsions between the negatively charged FA bound on graphene sheets imparted colloidal stability to the resulting graphene-FA composite (*Zeta* potential of −40 mV at pH = 7).

Demethylation of MeHg. The demethylation of MeHg was studied to determine the photocatalytic capacity of graphene-FA, as shown in Figure 3. Demethylation did not occur when MeHg was exposed to graphene. In addition to the zero band gap, aggregation is another inhibitor of photocatalytic activity, as depicted in Figure 2. For the first-order kinetics of the FA sample, the demethylation presented a rate constant of 0.0055 min^{-1} and a corresponding degradation half-life of 126 min. Previous work demonstrated that FA was converted to excited-state FA under UV light irradiation.[34] However, the rate constant was reduced to 0.0032 min^{-1}, corresponding to a degradation half-life of 217 min, when the FA sample was spiked with graphene. Thus, graphene acted as a quencher of excited molecules. Alternative explanations are that graphene may compete with FA for radiation absorption, or it may scatter radiation, thereby decreasing the irradiance available for FA. Interestingly, the self-assembled hybridized graphene-FA showed excellent demethylation activity with a rate constant of 0.0313 min^{-1} and a corresponding degradation half-life of 22.1 min, and the efficiency was approximately 5-fold higher than the efficiency of free FA with graphene. To investigate the photocatalytic capacity under visible light conditions, a subexperiment was conducted. The results are presented in Figure S5. The photocatalytic capacity decreased by 2 orders of magnitude compared to that under UVA conditions. Given its convenience, economy, and efficiency, the self-assembly of organic molecules is an ideal strategy for obtaining graphene-based catalysts. To investigate the stability and reusability of graphene-FA, graphene-FA was reused to treat methylmercury. As indicated by the results in Figure S6, there are no significant differences in the demethylation of methylmercury when reusing graphene-FA 10 or fewer times. This initial test demonstrates that graphene-FA is relatively stable and reusable.

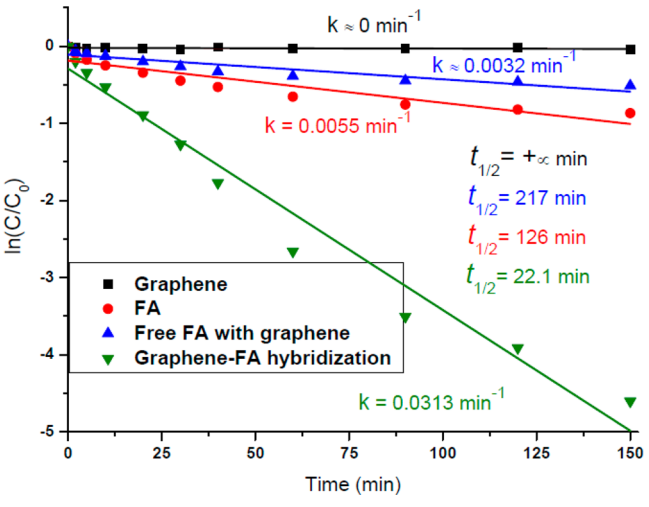

Figure 3. Rate of demethylation of MeHg by graphene, FA, free FA with graphene, and self-assembled hybridized graphene-FA. C_0 and C are the concentrations of MeHg before and after irradiation, respectively. The relative standard deviation ranged from 7% to 16%.

Identifying the Demethylation Products. Although the demethylation of MeHg has been reported using different methods, the transformation of mercuric species in various phases is still obscure. The demethylation products can be found in the solid phase (catalysts) as a result of absorption, in the aqueous phase, or in the gas phase, as depicted in Figure 4.

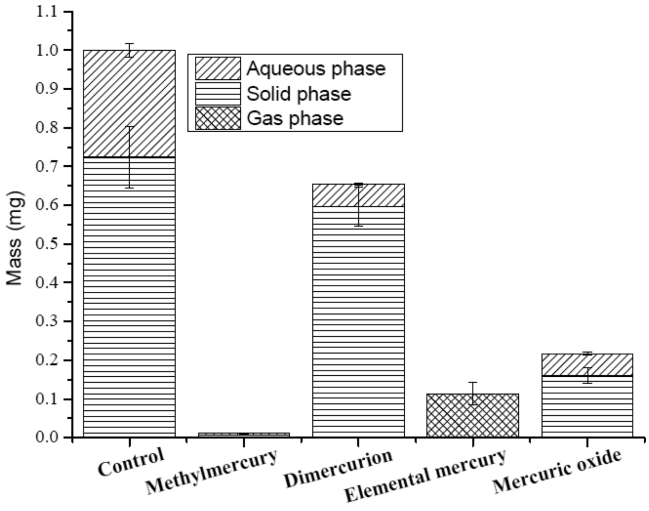

Figure 4. Demethylation products in the solid, aqueous, and gas phases after 150 min of irradiation using hybridized graphene-FA.

In the darkness control, 72.4% MeHg was absorbed on the catalyst. Hill et al. suggested that low-molecular-weight humic acids have a strong affinity for MeHg.[35] Therefore, it was hypothesized that a graphene-FA–methylmercury complex was the main product formed from MeHg under darkness. In contrast, more than 99% of MeHg was transformed into inorganic mercury after 150 min of irradiation. The main

dx.doi.org/10.1021/am501334j | ACS Appl. Mater. Interfaces 2014, 6, 9220–9227

photodegradation products were divalent mercury ions (65%), mercuric oxide (22%), and elemental mercury (12%). More than 70% of the divalent mercury ions and mercuric oxide were adsorbed on graphene-FA. Thus, the goal of recovering the inorganic mercury was achieved. Note that elemental mercury, which accounts for 12% of total mercury, could be released into the atmosphere and induce secondary contamination. The products of demethylation, such as elemental Hg, should be collected with great caution. The sulfurization of carbon materials was considered to be an effective method for removing elemental Hg.[36−38]

Demethylation Mechanisms. To verify the demethylation paths proposed above, the demethylation mechanisms were investigated. As depicted in Figure 5, dissolved oxygen

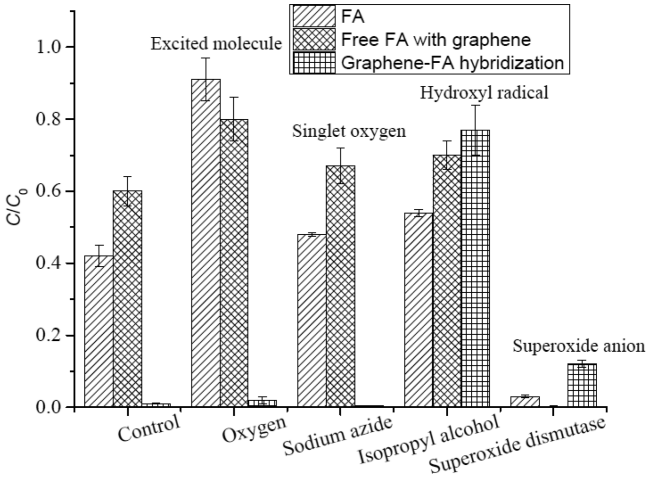

Figure 5. Effects of quenchers on the demethylation of MeHg using FA, free FA with graphene, and the self-assembled hybridized graphene-FA. The control is the experiment without quenchers. C_0 and C are the concentrations of MeHg before and after irradiation, respectively.

significantly inhibits demethylation using FA and free FA with graphene, whereas the quenchers sodium azide and isopropyl alcohol do not significantly inhibit demethylation, implying that excited-state FA rather than ROS is the main active species. Previous reports have also shown that FA is converted to excited-state FA under UV irradiation and that excited-state FA can catalyze the degradation of other molecules.[15] Interestingly, graphene acts as a quencher of excited-state FA and reduces demethylation, as shown in Figure 3. Until now, the quenching of FA or other excited-state molecules by graphene has remained unclear.[39] To elucidate the quenching mechanisms, the excited-state energy of FA and the energy level of graphene were calculated and compared. According to a previous report,[40] the excited-state energy of FA is 1.76−3.54 eV. Because the energy level of graphene is 4.42 eV,[41] excited-state FA can be quenched by electron transfer rather than by energy transfer, as shown in Figure 6.

Unlike FA or free FA with graphene, for the self-assembled hybridized graphene-FA, excited states contributed little to the demethylation, and hydroxyl radicals were the main reactive species, as shown in Figure 5. As is well-known, graphene is a material with a zero band gap, and it is not an excellent catalyst,[41] which is consistent with the information presented in Figure 3. Opening the band gap of graphene is a potential strategy to accelerate catalysis.[42] Figure 7a shows the square

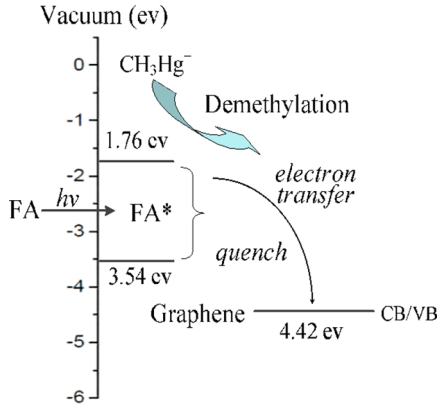

Figure 6. Quenching of excited-state FA by electron transfer to graphene. CB, conduction band; VB, valence band.

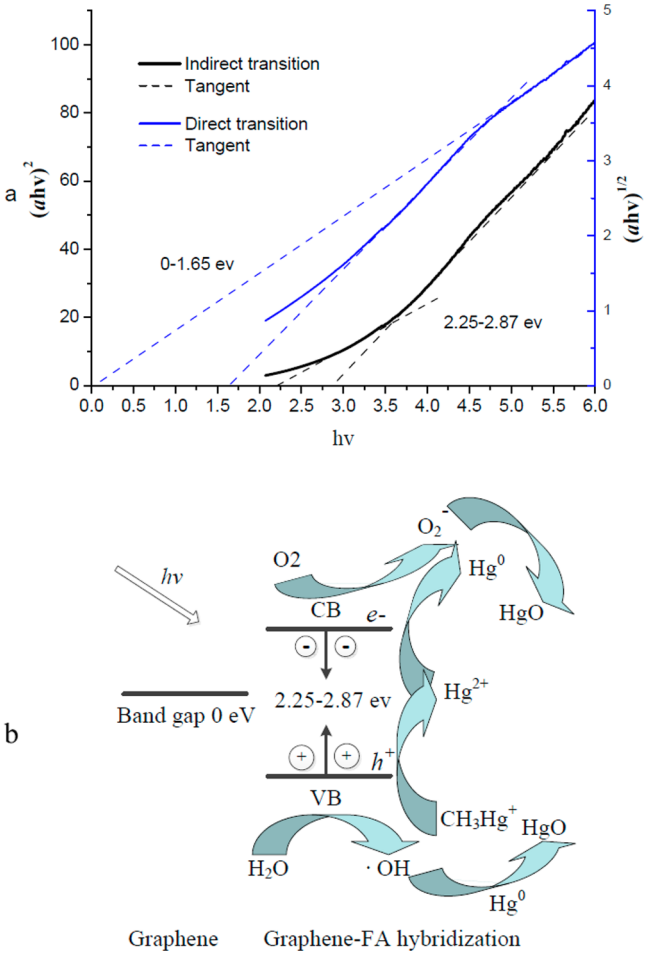

Figure 7. Mechanisms of demethylation using hybridized graphene-FA. FA opens the band gap of graphene (a), and demethylation is triggered by electron−hole separation (b). The generation of reactive species is confirmed in Figure 5.

and square root of the absorption energy ($\alpha h\nu$, where α is the absorbance of the UV optical absorption spectra) against photon energy ($h\nu$) to determine the energies for the indirect and direct transitions (band gap), respectively. Because graphene-FA includes FA molecules with various oxygenation levels, the converted plots did not show a sharp absorption edge for a precise energy gap. Figure 7a shows apparent energies of 0−1.65 and 2.25−2.87 eV for the direct and indirect

dx.doi.org/10.1021/am501334j | ACS Appl. Mater. Interfaces 2014, 6, 9220−9227

band gaps, respectively, in the graphene-FA specimen. Based on the threshold of the available wavelength (nm) = 1242.375/band gap, the available wavelength for an indirect band gap was 432.9−552.2 nm. Incident wavelengths lower than 432.9−552.2 nm likely induced separation of electron−hole pairs in graphene-FA. Photogenerated holes (h^+) migrated to the catalyst surface and reacted with water molecules adsorbed on the catalyst surface to produce OH. Photogenerated electrons, e^-, migrated to the catalyst surface, and molecular oxygen acted as an acceptor species in the electron-transfer reaction to produce O_2^-. Figure 5 confirms that ROS were generated by graphene-FA. The separation of electron−hole pairs and generation of ROS triggered the occurrence of demethylation, as depicted in Figure 7b. The recombination of electron−hole pairs will inhibit photocatalysis. As shown in Figure 6, FA is easily excited, and its electrons can be transferred to graphene. Herein, it was assumed that graphene is an electron reservoir and that FA is a photosensitizer. The electrons of the excited-state FA transferred to graphene, avoiding recombination with holes.

Toxicity Analysis. As shown in Figure 8, *Chlorella vulgaris* is very sensitive to graphene. The densities of microalgae in the graphene-exposed groups were significantly ($P < 0.05$) reduced compared to the density in the blank group. However, there were no remarkable differences between the graphene-FA and blank groups except for the high concentration exposure (50 mg/L). Graphene at 10 and 50 mg/L significantly inhibited the biosynthesis of chlorophyll a. This inhibition was only observed at 50 mg/L for graphene-FA. These results demonstrate that graphene-FA is more biocompatible than graphene. The probable reason for the enhanced biocompatibility of graphene-FA is that the immobilization of FA reduced the direct physical damage from graphene.[27]

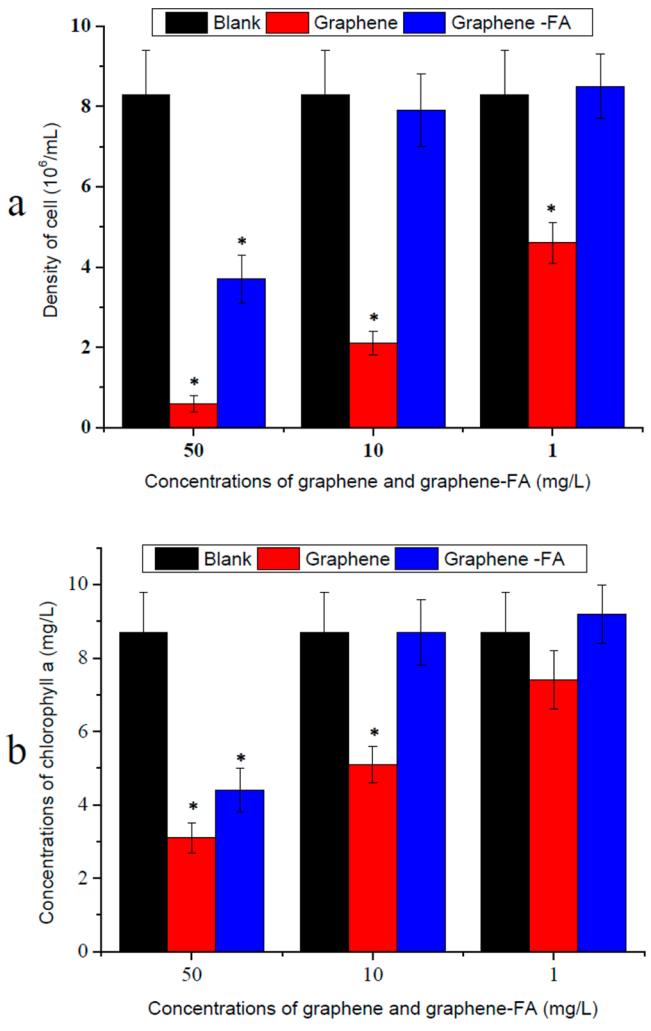

Figure 8. Toxicities of graphene and graphene-FA to *Chlorella*. (a) Effects of graphene and graphene-FA on the growth of *Chlorella*. (b) Effects of graphene and graphene-FA on the concentrations of chlorophyll a. The * represents the significance level ($P < 0.05$).

CONCLUSIONS

A novel chemical demethylation for methylmercury has been proposed. The low-toxicity graphene-FA was synthesized without the use of any chemical reagents. Graphene-FA presented an indirect open band gap of 2.25−2.87 eV with adequate aqueous dispersion. The immobilized FA accelerated the demethylation of mercury compared to free FA. The demethylation products and mechanisms were identified in the solid, aqueous, and gas phases. This work proposed that graphene acts as a quencher to the excited-state FA and inhibits the demethylation by electron transfer for the free FA with graphene. In contrast, the graphene in the self-assembled graphene-FA serves as an electron reservoir, causing separation of electron−hole pairs, which enhances the demethylation in which hydroxyl radicals are the main reactive species. Importantly, graphene-FA exhibited better biocompatibility than graphene. The results indicate that the green synthesis of graphene and organic molecules is a convenient strategy to obtain effective cocatalysts.

ASSOCIATED CONTENT

Supporting Information

Properties of graphene nanosheets. This material is available free of charge via the Internet at http://pubs.acs.org.

AUTHOR INFORMATION

Corresponding Author

*Tel.: +86-022-23507800. Fax: +86-022-23507800. E-mail: zhouqx@nankai.edu.cn.

Notes

The authors declare no competing financial interest.

ACKNOWLEDGMENTS

This work was financially supported by the National Natural Science Foundation of China (grant nos. 21037002, U1133006, and 21307061), the Tianjin Natural Science Foundation (grant no. 14JCQNJC08900), the Doctoral Program of Higher Education of China (grant no. 2013003112016), the Postdoctoral Science Foundation of China (grant no. 138528), and the Fundamental Research Funds for the Central Universities (grant no. 65121006).

REFERENCES

(1) Parks, J. M.; Johs, A.; Podar, M.; Bridou, R.; Hurt, R. A., Jr.; Smith, S. D.; Tomanicek, S. J.; Qian, Y.; Brown, S. D.; Brandt, C. C.; Palumbo, A. V.; Smith, J. C.; Wall, J. D.; Elias, D. A.; Liang, L. The Genetic Basis for Bacterial Mercury Methylation. *Science* **2013**, *339*, 1332−1335.

(2) Grandjean, P.; Satoh, H.; Murata, K.; Eto, K. Adverse Effects of Methyl-mercury: Environmental Health Research Implications. *Environ. Health Perspect.* **2010**, *118*, 1137−1145.

(3) Melamed, R.; da Luz, A. B. Efficiency of Industrial Minerals on the Removal of Mercury Species from Liquid Effluents. *Sci. Total Environ.* **2006**, *368*, 403−406.
(4) Khan, M. A. K.; Wang, F. Chemical Demethylation of Methylmercury by Selenoamino Acids. *Chem. Res. Toxicol.* **2010**, *23*, 1202−1206.
(5) Hu, X.; Mu, L.; Wen, J.; Zhou, Q. Covalently Synthesized Graphene Oxide-Aptamer Nanosheets for Efficient Visible-Light Photocatalysis of Nucleic Acids and Proteins of Viruses. *Carbon* **2012**, *50*, 2772−2781.
(6) Ie, I.-R.; Chen, W.-C.; Yuan, C.-S.; Hung, C.-H.; Lin, Y.-C.; Tsai, H.-H.; Jen, Y.-S. Enhancing the Adsorption of Vapor-Phase Mercury Chloride with an Innovative Composite Sulfur-Impregnated Activated Carbon. *J. Hazard. Mater.* **2012**, *217−218*, 43−50.
(7) Hsi, H. C.; Tsai, C. Y. Synthesis of TiO_{2-x} Visible-Light Photocatalyst Using N_2/Ar/He Thermal Plasma for Low-Concentration Elemental Mercury Removal. *Chem. Eng. J.* **2012**, *191*, 378−385.
(8) Hu, X. G.; Zhou, Q. X. Health and Ecosystem Risks of Graphene. *Chem. Rev.* **2013**, *113*, 3815−3835.
(9) Tang, H.; Yin, H.; Wang, J.; Yang, N.; Wang, D.; Tang, Z. Molecular Architecture of Cobalt Porphyrin Multilayers on Reduced Graphene Oxide Sheets for High-Performance Oxygen Reduction Reaction. *Angew. Chem., Int. Ed.* **2013**, *52*, 5585−5589.
(10) Yin, H.; Tang, H.; Wang, D.; Gao, Y.; Tang, Z. Facile Synthesis of Surfactant-Free Au Cluster/Graphene Hybrids for High-Performance Oxygen Reduction Reaction. *ACS Nano* **2012**, *6*, 8288−8297.
(11) Novoselov, K. S.; Falko, V. I.; Colombo, L.; Gellert, P. R.; Schwab, M. G.; Kim, K. A. Roadmap for Graphene. *Nature* **2012**, *490*, 192−200.
(12) Quhe, R.; Fei, R.; Liu, Q.; Zheng, J.; Li, H.; Xu, C.; Ni, Z.; Wang, Y.; Yu, D.; Gao, Z.; Lu, J. Tunable and Sizable Band Gap in Silicene by Surface Adsorption. *Sci. Rep.* **2012**, *2*, 853.
(13) Yin, H.; Zhao, S.; Wan, J.; Tang, H.; Chang, L.; He, L.; Zhao, H.; Gao, Y.; Tang, Z. Three-Dimensional Graphene/Metal Oxide Nanoparticle Hybrids for High-Performance Capacitive Deionization of Saline Water. *Adv. Mater.* **2013**, *25*, 6270−6276.
(14) Kim, M.-K.; Zoh, K.-D. Effects of Natural Water Constituents on the Photo-Decomposition of Methylmercury and the Role of Hydroxyl Radical. *Sci. Total Environ.* **2013**, *449*, 95−101.
(15) Fan, C.; Horng, C.-Y.; Li, S.-J. Structural Characterization of Natural Organic Matter and Its Impact on Methomyl Removal Efficiency in Fenton Process. *Chemosphere* **2013**, *93*, 178−183.
(16) Zong, G.; Chen, H.; Qu, R.; Wang, C.; Ji, N. Synthesis of Polyacrylonitrile-Grafted Cross-Linked N-Chlorosulfonamidated Polystyrene via Surface-Initiated ARGET ATRP, and Use of the Resin in Mercury Removal after Modification. *J. Hazard. Mater.* **2011**, *186*, 614−621.
(17) Wiatrowski, H. A.; Das, S.; Kukkadapu, R.; Ilton, E. S.; Barkay, T.; Yee, N. Reduction of Hg(II) to Hg(0) by Magnetite. *Environ. Sci. Technol.* **2009**, *43*, 5307−5313.
(18) Zachariadis, G. A.; Kapsimali, D. C. Effect of Sample Matrix on Sensitivity of Mercury and Methylmercury Quantitation in Human Urine, Saliva, and Serum Using GC-MS. *J. Sep. Sci.* **2008**, *31*, 3884−3893.
(19) Jacobs, L. E.; Fimmen, R. L.; Chin, Y.-P.; Mash, H. E.; Weavers, L. K. Fulvic Acid Mediated Photolysis of Ibuprofen in Water. *Water Res.* **2011**, *45*, 4449−4458.
(20) Bagri, A.; Mattevi, C.; Acik, M.; Chabal, Y. J.; Chhowalla, M.; Shenoy, V. B. Structural Evolution During the Reduction of Chemically Derived Graphene Oxide. *Nat. Chem.* **2010**, *2*, 581−587.
(21) Zhao, M.; Deng, K.; He, L.; Liu, Y.; Li, G.; Zhao, H.; Tang, Z. Core-Shell Palladium Nanoparticle@Metal-Organic Frameworks as Multifunctional Catalysts for Cascade Reactions. *J. Am. Chem. Soc.* **2014**, *136*, 1738−1741.
(22) Abakumov, E. V.; Cajthaml, T.; Brus, J.; Frouz, J. Humus Accumulation, Humification, and Humic Acid Composition in Soils of Two Post-Mining Chronosequences after Coal Mining. *J. Soils Sediments* **2013**, *13*, 491−500.
(23) Akhavan, O.; Ghaderi, E. Toxicity of Graphene and Graphene Oxide Nanowalls Against Bacteria. *ACS Nano* **2010**, *4*, 5731−5736.
(24) Patil, A. J.; Vickery, J. L.; Scott, T. B.; Mann, S. Aqueous Stabilization and Self-assembly of Graphene Sheets into Layered Bionanocomposites using DNA. *Adv. Mater.* **2009**, *21*, 3159−3164.
(25) Okpalugo, T. I. T.; Papakonstantinou, P.; Murphy, H.; McLaughlin, J. High Resolution XPS Characterization of Chemical Functionalised MWCNTs and SWCNTs. *Carbon* **2005**, *43*, 153−161.
(26) Penicaud, A.; Drummond, C. Deconstructing Graphite: Graphenide Solutions. *Acc. Chem. Res.* **2013**, *46*, 129−137.
(27) Liu, S.; Zeng, T. H.; Hofmann, M.; Burcombe, E.; Wei, J.; Jiang, R.; Kong, J.; Chen, Y. Antibacterial Activity of Graphite, Graphite Oxide, Graphene Oxide, and Reduced Graphene Oxide: Membrane and Oxidative Stress. *ACS Nano* **2011**, *5*, 6971−6980.
(28) Chen, K. L.; Elimelech, M. Aggregation and Deposition Kinetics of Fullerene (C_{60}) nanoparticles. *Langmuir* **2006**, *22*, 10994−11001.
(29) Jouraiphy, A.; Amir, S.; Winterton, P.; El Gharous, M.; Revel, J. C.; Hafidi, M. Structural Study of the Fulvic Fraction During Composting of Activated Sludge-Plant Matter: Elemental Analysis, FTIR and C^{13} NMR. *Bioresour. Technol.* **2008**, *99*, 1066−1072.
(30) Semsarilar, M.; Jones, E. R.; Blanazs, A.; Armes, S. P. Efficient Synthesis of Sterically-Stabilized Nano-Objects via RAFT Dispersion Polymerization of Benzyl Methacrylate in Alcoholic Media. *Adv. Mater.* **2012**, *24*, 3378−3382.
(31) Sheng, G.; Li, J.; Shao, D.; Hu, J.; Chen, C.; Chen, Y.; Wang, X. Adsorption of Copper(II) on Multiwalled Carbon Nanotubes in the Absence and Presence of Humic or Fulvic Acids. *J. Hazard. Mater.* **2010**, *178*, 333−340.
(32) Mann, J. A.; Rodriguez-Lopez, J.; Abruna, H. D.; Dichtel, W. R. Multivalent Binding Motifs for the Noncovalent Functionalization of Graphene. *J. Am. Chem. Soc.* **2011**, *133*, 17614−17617.
(33) Chen, J.; Chen, W.; Zhu, D. Adsorption of Nonionic Aromatic Compounds to Single-Walled Carbon Nanotubes: Effects of Aqueous Solution Chemistry. *Environ. Sci. Technol.* **2008**, *42*, 7225−7230.
(34) Berkovic, A. M.; Bertolotti, S. G.; Villata, L. S.; Gonzalez, M. C.; Pis Diez, R.; Martire, D. O. Photoinduced Reduction of Divalent Mercury by Quinones in the Presence of Formic Acid under Anaerobic Conditions. *Chemosphere* **2012**, *89*, 1189−1194.
(35) Hill, J. R.; O'Driscoll, N. J.; Lean, D. R. S. Size Distribution of Methylmercury Associated with Particulate and Dissolved Organic Matter in Freshwaters. *Sci. Total Environ.* **2009**, *408*, 408−414.
(36) Feng, W.; Borguet, E.; Vidic, R. D. Sulfurization of Carbon Surface for Vapor Phase Mercury Removal - I: Effect of Temperature and Sulfurization Protocol. *Carbon* **2006**, *44*, 2990−2997.
(37) Ho, T. C.; Shetty, S.; Chu, H. W.; Lin, C. J.; Hopper, J. R. Simulation of Mercury Emission Control by Activated Carbon under Confined-Bed Operations. *Powder Technol.* **2008**, *180*, 332−338.
(38) Hsi, H.-C.; Tsai, C.-Y.; Kuo, T.-H.; Chiang, C.-S. Development of Low-Concentration Mercury Adsorbents from Biohydrogen-Generation Agricultural Residues Using Sulfur Impregnation. *Bioresour. Technol.* **2011**, *102*, 7470−7477.
(39) de Miguel, M.; Alvaro, M.; Garcia, H. Graphene as a Quencher of Electronic Excited States of Photochemical Probes. *Langmuir* **2012**, *28*, 2849−2857.
(40) Canonica, S.; Jans, U.; Stemmler, K.; Hoigne, J. Transformation Kinetics of Phenols in Water: Photosensitization by Dissolved Natural Organic Material and Aromatic Ketones. *Environ. Sci. Technol.* **1995**, *29*, 1822−31.
(41) Lee, J. S.; You, K. H.; Park, C. B. Highly Photoactive, Low Bandgap TiO_2 Nanoparticles Wrapped by Graphene. *Adv. Mater.* **2012**, *24*, 1084−1088.
(42) Yeh, T.-F.; Chan, F.-F.; Hsieh, C.-T.; Teng, H. Graphite Oxide with Different Oxygenated Levels for Hydrogen and Oxygen Production from Water under Illumination: The Band Positions of Graphite Oxide. *J. Phys. Chem. C* **2011**, *115*, 22587−22597.